# WIND-TUNNEL TESTING OF V/STOL CONFIGURATIONS AT HIGH LIFT

W. R. Sears
University of Arizona, Tucson, Arizona

## Abstract

It is argued that the adaptive-wall wind-tunnel scheme offers a way to solve a persistent problem of V/STOL testing, namely interference of tunnel boundaries with the powered, vortical wake at large lift coefficients. First, it is shown that the adaptable-wall scheme permits the simulated free-stream direction to be chosen independently of wind-tunnel architecture. It is also found that the wake can be allowed to pass downstream without encountering the interface defined by the instrument-array of the tunnel. The combination of these two ideas leads to a new type of wind tunnel - the "Arizona V/STOL Tunnel" - in which the model's orientation and the free-stream vector are chosen to put the wake in the desired position and simulation of the correct free-stream vector, defining the desired angle of attack, is achieved by means of the adaptable-wall iterative strategy.

To facilitate a numerical demonstration of this kind of tunnel, a simple panel model of a jet-flap wing and wake is constructed, suitable for the non-linear, high-lift regime and for the inclusion of wind-tunnel effects. Using this model, step-by-step, numerical simulation of the testing of this jet-flap wing in the new tunnel is undertaken. The wall-control organs of the adaptable walls are modelled as uniform source panels, 28 in all. The simulation is rather involved, requiring iterations of the wing/wake model within the iterative scheme of the adaptable-wall tunnel, but computer costs are trivial. Convergence is obtained and the final wing/wake properties are close to unconfined-flow values for the same wing-model, even though starting conditions were grossly different from preselected final conditions.

## Table of Notation

| | |
|---|---|
| $C$ | jet-momentum coefficient |
| $f,g$ | flow variables (functions) used to establish unconfined flow in the adaptable-wall scheme |
| $g[f]$ | the function g according to the computed outer flow determined by boundary values f and the far-field boundary conditions |
| $k$ | "relaxation factor" defined in Table I, Steps 4 and 6, and Eq. (2) |
| $S$ | the interface between inner and outer flow regions |
| $q$ | strength of source-panel on $\Sigma$ |
| $u,v,w$ | Cartesian components, in the x,y,z coordinate system, of the perturbation velocity vector viz., (u,v,w) = (fluid velocity) - $\vec{U}$ |
| $\vec{U}$ | simulated free-stream vector |
| $U$ | magnitude of $\vec{U}$ |
| $v_t$ | tangential (to S) component of (u,v,w) |
| $v_n$ | normal (to S) component of (u,v,w) |
| $V_{n_{ij}}$ | matrix giving $v_n$ at point i due to unit increase of strength of j-th panel, including indirect effect due to model |
| $V_{t_{ij}}$ | same for $v_t$ |
| $x,y,z$ | Cartesian coordinate system (Fig. 1); the x-direction is parallel to the tunnel axis |
| $\alpha$ | angle of attack |
| $\Gamma$ | circulation; thus $\Gamma_r$ = strength of r-th dipole panel of the jet-flap model |
| $\delta f, \delta v_n$ | mismatch signal defined in Table I, Step 4 |
| $\Delta q$ | increment in source strength q (See Table IV) |
| $\theta$ | inclination of wake panel relative to tunnel axis |
| $\Sigma$ | surface formed by wall-control panels - "the tunnel wall" |

### Subscripts

| | |
|---|---|
| $i$ | field-point number (point on S) |
| $j$ | panel number (panel on $\Sigma$) |
| $n$ | normal |
| $t$ | tangential |
| $G$ | point G, the midpoint of the transverse vortex segment of a plane horseshoe vortex |
| $r$ | panel number (panel of wing/wake model) |

### Superscripts

| | |
|---|---|
| $(p)$ | denotes quantities pertaining to the p-th iteration |

## I. Introduction

The special problem posed by the wind-tunnel testing of V/STOL configurations is that they produce very large lift coefficients and therefore large deflections of the airstream. Thus, whereas the regime of flight at very low forward speeds - the "transition" regime - is typically the most important in the wind-tunnel schedule, it is also the one exhibiting the greatest flow deflections and posing the most serious problems for the wind-tunnel operator. Testing in this regime requires accurate simulation of energized, vortical wakes that are strongly directed downward and are often grossly distorted by the tunnel boundaries, including the floor.

The present paper reports on studies carried out at the University of Arizona, under sponsorship of the U.S. Office of Naval Research, intended to solve this problem by exploitation of the concept of adaptive wind-tunnel walls.

We begin with a short review of this concept and argue that it eliminates, along with boundary interference, the inaccuracies of the usual tunnel calibration. We then proceed to describe some numerical models of adaptive-wall tunnels, showing, in particular, that the undisturbed-stream direction and magnitude, arbitarily chosen, are achieved by the iterative process of such a tunnel.

The evidence resulting from these simulations leads to a new idea in V/STOL testing, in which flow geometry is chosen to obviate the problem of the wake, and the simulated stream direction is divorced from the architecture of the tunnel and attained by the adaptive-wall strategy.

Next, to demonstrate the use of this type of tunnel in an extreme case, a numerical model of a representative powered-lift wing in a strongly nonlinear regime is needed. An approximate panel representation of a jet-flap wing of finite span is therefore constructed. Finally, the testing of such a wing in this kind of tunnel is modelled; i.e., the iterative process by which this wing is brought from an arbitrary initial situation to the desired unconfined-flow condition is simulated in detail. This demonstration, while somewhat tedious, is completely successful, suggesting that the new tunnel would solve the recurring problem of V/STOL testing.

## II. The Adaptive-Wall Concept

The idea of a wind tunnel whose working-section walls are modified during each experiment so as to produce, for whatever configuration may be under test, an exact simulation of flight conditions originated in the early 1970's[1,2], has been discussed for some years now, and would not seem to require detailed presentation in this paper. Nevertheless, a brief summary may be helpful to readers.

The scheme requires (a) that the working-section walls be provided with control organs such that their shape, porosity, and/or exterior plenum pressures can be modified, and (b) that instrumentation be provided within the working section to measure certain flow variables with the model in place. This instrumentation defines a surface S, surrounding the model, and measures the required flow variables at (in principle) all points of S. The wall-control organs must be capable of controlling flow conditions on S, and are iteratively adjusted to produce unconfined-flow conditions there.

The third necessary feature of an adaptable-wall tunnel is (c) capability to calculate the flow field external to S - i.e., computing hardware and software to model numerically, for given boundary data on S, this external flow field including its appropriate far-field boundary conditions. The surface S is therefore the interface between the flow-field actually produced inside S with model in place, engines running, etc., and the calculated exterior flow field that satisfies the far-field conditions but, of course, exists only within the computer.

In practice, the adjustment to unconfined flow is accomplished as follows:
1. Two flow variables, say $f^{(1)}$ and $g^{(1)}$, are measured on S. Clearly, these are either consistent with the required far-field conditions, or they are not. In other words, either of these measured functions is adequate, together with far-field conditions, to define an exterior flow field; in this sense the other measured function is redundant.
2. One of these functions, say $f^{(1)}$, is used as boundary data on S and the corresponding external field is calculated, satisfying far-field conditions. The other variable, say $g[f^{(1)}]$, is read out from this calculation and is compared with the measured function $g^{(1)}$. The difference $g[f^{(1)}]-g^{(1)}$, which we call $\delta^{(1)}g$, measures the degree of mismatch at the interface.
3. The wall-control organs are adjusted so as to add a fraction of $\delta^{(1)}g$, say $k\delta^{(1)}g$, where $0<k<1$, to the previously measured values $g^{(1)}$ on S. New distributions $f^{(2)}$ and $g^{(2)}$, presumably improved, are measured, the computations in Step 2 are repeated, and so on until the function $\delta g$ is as small as desired - or as small as can be achieved in a given experiment. If $\delta g$ is zero, the inner and outer flows match on S and the matched flow satisfies all the boundary conditions; the flow in the tunnel is a correct representation of unconfined flow.

This process is summarized in Table I.

The adaptive-wall scheme has now been demonstrated

Table I

Outline of the Adaptable-Wall Iteration

1. Set model configuration ($\alpha$, flap angles, power, etc.) and initial tunnel configuration (arbitrary).
2. Measure $f^{(1)}$ and $g^{(1)}$ on interface S.
3. Calculate outer flow-field with $f^{(1)}$ as boundary values and read out $g[f^{(1)}]$.
4. Form $\delta^{(1)}g = g[f^{(1)}] - g^{(1)}$ and $g^{(2)} = g^{(1)} + k\delta^{(1)}g$.
5. Adjust wall-control organs to obtain $g = g^{(2)}$ on S.
6. Repeat from Step 2: ($g^{(n+1)} = g^{(n)} + k\delta^{(n)}g$ etc.) until $\delta^{(n)}g$ is as small as required.

successfully, both in real wind tunnels and in numerical simulation, in a number of laboratories, principally in the regime of transonic flow speeds[3,4].

## III. Determination of Free-Stream Vector

In these studies and experiments, emphasis has typically been put on elimination of wall interference and not on questions of tunnel calibration. It has not always been appreciated that the adaptive-wall technique essentially eliminates the need for speed calibration and also removes the possiblity of errors in "undisturbed-flow direction".

Errors in both the speed calibration and the simulated undisturbed-flow direction are probably present in most wind tunnels when large and/or high-lift models are tested. The undisturbed-stream vector $\vec{U}$ is a fictitious value that does not actually occur anywhere in a typical wind-tunnel test. According to the tunnel's speed-calibration curves, the flow speed U would obtain in the empty working section if the appropriate manometer pressure-difference were maintained. The effect of the model on this calibration is not usually known, but is assumed to be small. As regards the simulated flow direction the situation is even more uncertain: care is taken to assure that the empty-tunnel flow is accurately parallel to the drag direction of the balance system - e.g. horizontal - but there is little reason to believe that the simulated vector $\vec{U}$ therefore has the same direction when a large model is being tested.

Unfortunately, it is of primary importance to know $\vec{U}$ accurately in both magnitude and direction. For example, since the force on a model is decomposed into lift and drag by the balances, any error in flow direction, arg $\vec{U}$, results in large errors in drag, specifically an error of the amount $L \cdot \Delta\theta$, where L is the lift and $\Delta\theta$ is the error in simulated flow direction. Thus, errors $\Delta\theta$ of about 0.1 degree (.0017 radian) make significant errors in measured drag for many cruise configurations!

In an adaptive-wall tunnel the stream vector $\vec{U}$ is selected by the operator and put into the exterior-flow calculation. The process of iteration to unconfined flow then leads, in principle, to correct simulation in the tunnel at this stream magnitude and direction, provided only that the instrumentation ((b) above) and exterior-flow computation ((c) above) are sufficiently accurate and the wall-control mechanism ((a) above) is adequate to provide conditions demanded by the iterative algorithm.

To be sure, the need for high accuracy in the determination of the vector $\vec{U}$, pointed out here, probably pertains more to tests at long-range cruise conditions than to the high-lift, V/STOL transition regime that is the primary concern of this paper. Nevertheless, as will be shown, the ability of the tunnel operator to select $\vec{U}$ at will in an adaptive-wall tunnel is essential in solving the V/STOL problem.

## IV. Numerical Studies of V/STOL Wind Tunnels

Our studies at the University of Arizona have involved simulation, by panel methods, of incompressible flow about lifting wings in rectangular working sections. It may be useful to remind the reader at this point that "numerical simulation" here means that the processes of flow modification by means of wall elements and of measurement of flow properties on S are modelled numerically, while the calculation of exterior flow and the process of iteration are carried out exactly as they would be in practice if the tunnel existed. Of course, a wing and its response to flow in the tunnel must also be modelled.

In view of the large flow deflection expected, it was believed necessary to use an interface S that enclosed the wing and to control flow conditions at its upstream (and, perhaps, downstream) face. It will be recognized that the exterior-flow calculation, both in these simulations and in actual operation of a wind tunnel, would be greatly complicated by a wake emerging from S into the exterior-flow region. Early in the program, therefore, numerical experiments were carried out to resolve this matter. These confirmed that such a vortical wake did indeed make the calculation difficult, but that the difficulties could be eliminated by extending the interface S downstream so far that the wake did not penetrate it.

The tunnel configuration thus arrived at is sketched in Figure 1. In it, the interface S is square in cross-section, closed upstream, and extends indefinitely downstream. For the exterior-flow calculation, the four sides of S are made up of rectangular panels of constant distributed-vortex strength. These are the singularity-panels commonly used in aerodynamic studies, in which the transverse vortex strength ($\gamma_y$ or $\gamma_z$) is uniform while $\gamma_x$ is concentrated in line vortices at the

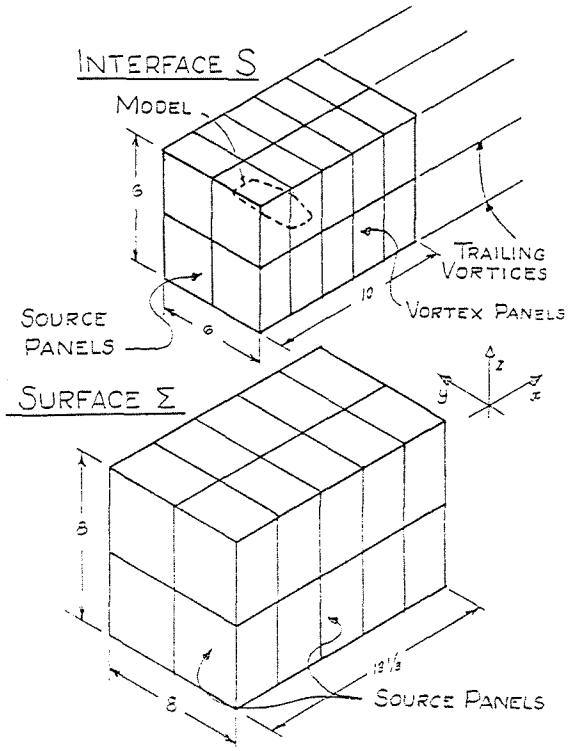


FIGURE 1
Panel arrays (interface S and tunnel walls Σ) and coordinate system

lateral edges of the panels. Since these vortices extend indefinitely in the x direction, the interface can be said to be infinite in extent. The front face of S is made up of source panels of constant strength. There is a single measurement-station ("field point") at the midpoint of each panel of S.

This semi-infinite interface S is enclosed in another, larger, rectangular array of uniform-source panels, $\Sigma$, as shown; this represents the array of control organs at the walls of a tunnel. Experience shows that flow conditions at the field points of S can be contolled to adequate degree (as will be shown below) by this five-sided rectangular array. The two flow quantities f and g are chosen to be the tangential and normal components of the perturbation velocity vector, $v_t$ and $v_n$. In terms of Cartesian components u,v,w we take $v_t$ to be w on the upstream face of S and u on the sides, top, and bottom; $v_n$, of course, is u on the upstream face, v on the sides, and w on top and bottom. (The panels of S and $\Sigma$ were designed to be used with these choices for f and g). As indicated in our Table of Notation, the perturbation vector is always defined relative to the specified, desired, free-stream velocity vector.

Initial numerical experiments using arrays of this kind, with various numbers of panels, were made with a "responsive" horseshoe-vortex wing in the tunnel. This nomenclature denotes a horseshoe vortex, lying in the xy-plane, whose circulation $\Gamma$ is linearly related to the velocity components u and w at the midpoint of its transverse segment (point G). For example, if the stream vector is $\vec{U} = (1,0,0)$, we put

$$\Gamma = \frac{\pi}{2}\{1 + u_G + 2w_G\} \qquad (1)$$

where $u_G$ and $w_G$ are perturbation velocity components, relative to $\vec{U}$, at point G. This can be interpreted as the circulation about a wing of unit chord whose effective incidence is 1/2 radian. The span of the horseshoe is 4 units, which is half of the width and height of $\Sigma$.

With this very simple wing-model, the adaptive-wall process was carried out for a variety of initial conditions including wall interference (extraneous velocity perturbations) and errors in $\vec{U}$, using various arrangements of panels on S and $\Sigma$, and various values of the relaxation factor k.

An essential step in this modelling (as it is in real operation of an adaptive tunnel) is to determine the strengths of the panels of $\Sigma$, representing the setting of wall-control organs, to change the flow variable g (viz. $v_n$) at S by the chosen amount $k\delta g$ in any given iteration. Now, for incompressible irrotational flow and a linear wing-model, the values of $v_n$ are linearly related to the source strengths of $\Sigma$-panels; the calculation is therefore a simple inversion of the matrix that expresses the influence of the $\Sigma$-panels on $v_n$ at field-points of S. But the matrix must include both the direct influence of the $\Sigma$-panels at the field points and the indirect effect, namely the effects at the field points caused by the effects of $\Sigma$-panels on the wing, i.e., on its circulation. We call this the "combined matrix". Similarly, of course, the values of f (viz. $v_t$) that result from the adjustment of $\Sigma$-panel strengths must also be calculated by means of a combined $v_t$-matrix.

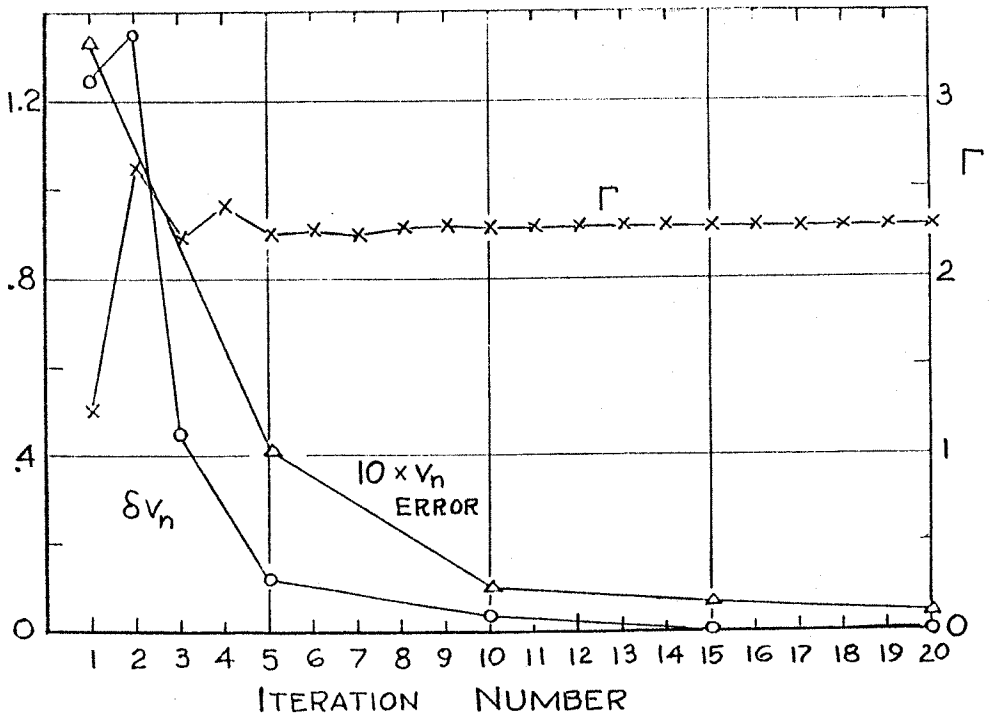


FIGURE 2 - Iteration of responsive horseshoe-vortex wing to unconfined flow in wind tunnel. k = 0.25. Initial condition: $\vec{U}$ = 0.8 at zero inclination, with wall interference. Final condition: $\vec{U}$ = 1.0 at 0.25 radian, unconfined flow. x Circulation $\Gamma$ (r.h. scale). o Maximum $\delta v_n$ on S (1.h. scale). $\Delta$ Average absolute true error in $v_n$ on S (1.h.scale). (The points are connected only for clarity).

When the number of panels on $\Sigma$ is the same as the number of field-points on S, these calculations involve square matrices and are straight-forward. It is desirable, however, to have more field points than $\Sigma$-panels; in this case the source strengths on $\Sigma$ are determined by a least-square-error procedure that gives a best fit to the up-dated $v_n$-vector.

Figure 2 presents a typical result of these studies, namely the results of a run made to demonstrate the ability of this model tunnel to produce an arbitrarily selected stream vector $\vec{U}$. The desired stream vector was chosen to be of unit magnitude at an angle of 1/4 radian to the x-axis. The initial condition, as indicated, was assumed to involve an erroneous stream vector as well as conventional wall interference, represented here by "image" horseshoe vortices reflected in the tunnel walls. As indicated above, the arrays $\Sigma$ and S are again aligned with the x-axis; the horseshoe-vortex wing also lies in the xy-plane. Eq. (1), for $\Gamma$, was modified appropriately for this calculation, since the unconfined flow now involves a different stream vector; the unconfined-flow value of $\Gamma$ for this case is 2.30 in the units used here.

As Figure 2 shows, convergence to unconfined flow at the desired stream condition was obtained. Three quantities are plotted against the iteration number: (i) the circulation $\Gamma$, (ii) the maximum value of $|\delta v_n|$ on S, and (iii) the absolute true error in $v_n$ averaged over the field points of S. This third quantity, the "true error" defined in (iii), may require some explanation: In this particular case the exact flow field of the horseshoe-vortex wing with circulation 2.30 is, of course, known. The converged values of $v_n$ at the field points of S can therefore be compared with these exact values and the absolute error evaluated. It is, clearly, not the same as $\delta v_n$, since $\delta v_n$ is the difference between inner and outer flows, both modelled by rather crude numerical methods. If $\delta v_n$ were exactly zero, this true error would still not necessarily vanish, and would measure the ultimate ability of the chosen $\Sigma$-panel array to simulate unconfined horseshoe-vortex flow.

The value of k, the relaxation constant, was 0.25 in this run. As predicted above, there is measurable error in the final, converged flow field, as indicated by the average "true error", but it is less than one percent of the stream speed. Figure 2 is typical of many trials made with the "responsive horseshoe-vortex" wing with various initial conditions, especially errors in stream magnitude and/or direction and various final conditions.

## V. The Arizona V/STOL Wind Tunnel

At this point we have presented evidence suggesting (A) that the adaptive-wall scheme permits the stream direction and magnitude to be chosen independently of the geometry of the wind tunnel and (B) that the difficulties posed by the wake can be avoided if the wake does not emerge from the interface S. Together, these conclusions lead to the concept of a new kind of wind tunnel, in which model attitude is chosen to conform to (B) and simulated stream direction is then chosen to produce the desired angle of attack as in (A). This constitutes the "Arizona V/STOL Tunnel", or AVT.

Since our objective is to accommodate cases where the wake is grossly deflected from the stream direction, and since the interface must lie within the tunnel, it seems clear that the architecture of the tunnel must be divorced from the stream direction. In particular, there must be provision for strong vertical cross-flow in the tunnel up- and downstream of the model. A rough, conceptual sketch of an AVT is presented in Figure 3. We presume that a variable-angle nozzle upstream would provide the conditions required there, without excessive turbulence. The nozzle angle would constitute one of the control organs of the adaptable-wall scheme, as would the tunnel's speed control. We assume that the conditions required downstream of the model can best

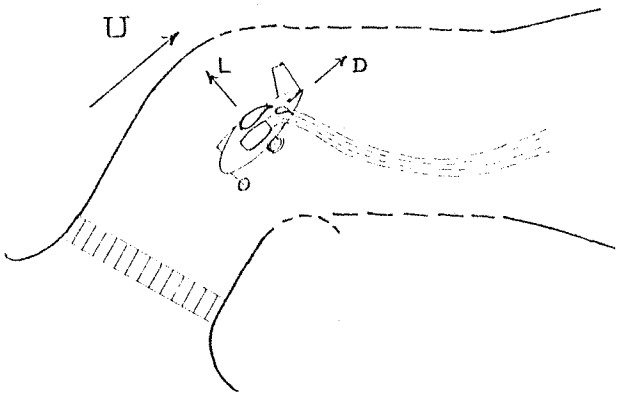


FIGURE 3
Sketch of a proposed wind tunnel of the AVT type

Table II

Outline of AVT Procedure

1. Set model configuration: flap angles, power, etc.
2. Set initial tunnel configuration and approximate speed.
3. Rotate model so that wake trails downstream without impinging on instrumentation defining S.
4. Choose stream vector $\vec{U}$ to give desired angle of attack, and begin iteration to unconfined flow, as outlined in Table I.
5. If wake changes position sufficiently to interfere with S, rotate model and stream vector equal amounts and proceed with iteration.

be achieved by control of wall porosity and/or pressure in subdivided plenum chambers, and that turbulence may be less critical here than upstream.

In any case, the operating procedure for this type of tunnel will be unlike that of conventional tunnels. To run a test at a given angle of attack $\alpha$, it will be necessary to guess at a free-stream direction and model orientation, their difference being $\alpha$, that will put the wake properly within S. (It should be easy to provide simple total-head or pitot-static tubes to ascertain roughly the wake position).

To be sure, the wake position is affected by all other variables and may change during adjustment of the adaptable walls. The sequence of events appears to be that outlined in Table II.

The next objective of this investigation is to demonstrate, by numerical simulation, that a tunnel of the AVT category can, in fact, be brought to unconfined-flow conditions with a powered-lift model in place at a large lift coefficient. For this purpose, a rectangular tunnel-model similar to the one described and used above will be employed, but it is necessary to provide a simple, suitable, high-lift wing model as well.

## VI. A Simple Jet-Flap-Wing Model

The jet-flap wing is an attractive example, since it can be modelled rather simply. Its theory has been presented in References 5-8. A numerical representation suitable for nonlinear, large-deflection cases is given in Reference 9, and a panel method for high-lift conventional wings is given in Reference 10.

Here we use the array of dipole panels (rectangular vortex rings) sketched in Figure 4. There are 16 panels of constant dipole strength; 8 represent the wing and its mechanical flap and therefore have specified angles of incidence; the remaining 8 represent the momentum-wake, whose shape is unknown and must be determined.

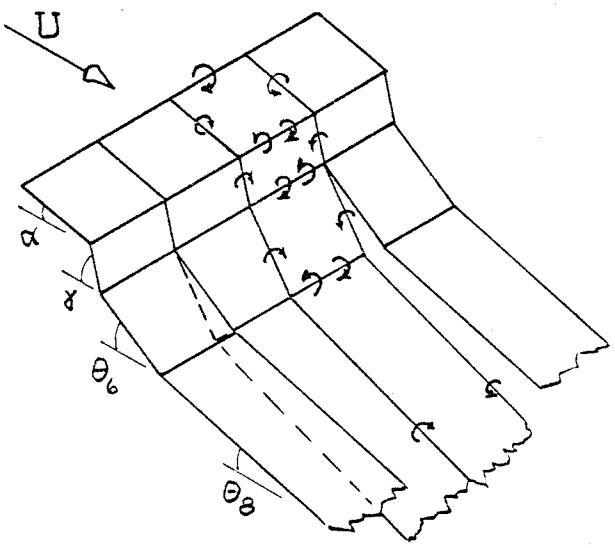


FIGURE 4 - Sketch showing panel model of jet-flap wing and wake

Two wake conditions determine this shape:

I. The wake is impermeable; thus the total normal velocity component - here evaluated at a single selected field-point on each panel - must vanish.

II. The normal force on the wake is proportional to the jet momentum flux and the wake curvature.

In the present approximation, wake circulation is concentrated in vortex filaments at the lines where the panels join. The force is therefore concentrated there too, and produces finite angular deflections there. We neglect the lateral velocity components at the wake panels; they also affect the wake shape, but the vertical deflection of the wake is much larger near the wing, and therefore more important.

It will be recognized that the unknowns here are the 16 panels strengths $\Gamma_r$ and 8 wake-panel angles $\theta_r$. These are determined by 16 kinematic conditions (I, above) and 8 force conditions (II). For large deflections (high lift), these relations are nonlinear. We obtain a solution, for a given wing and given jet-momentum flux, by assuming that the changes of wake deflections from one iteration to the next are small angles; this permits linearization of the trigonometric functions involved. Other quantities involved in conditions I and II are flow-field quantities and are evaluated from the preceding iteration. In other words, the solution is obtained by local linearization at each step, assuming small change of wake deflection in the next step. This technique requires that a guess be made for the $\theta_r$'s to get the process started. The calculation at each step is then the solution of a set of linear algebraic equations, for which rapid matrix techniques are available.

Before this model was used in our wind-tunnel studies, it was exercised in cases of unconfined flow at various angles of attack and jet-momentum coefficients. The Cyber 175 computer at the University of Arizona was used. The effects of increasing the number of panels, both laterally and longitudinally, was also investigated. It was found that 10 to 15 iterations were required to reach convergence in unconfined flow. In the interests of brevity, further details concerning the jet-flap-wing model will not be presented here; interested readers are referred to Reference 11.

## VII. Simulation of a Test of the Jet-Flap-Wing in the AVT

We now propose to demonstrate that a tunnel of the AVT type can be used to produce unconfined conditions around a jet-flap wing of the kind just described, at very large lift coefficients and large wake deflections, when the initial conditions are far from those desired. As already mentioned, the tunnel is modelled by a rectangular panel array similar to that used previously. Thus, although we have in mind a tunnel like the one sketched in Figure 3, for example, we do not attempt to model its upstream geometry in detail. Rather, we assume that the rectangular panel arrays, $\Sigma$ and S of Figure 1, represent a category of AVT tunnels having instrumentation to measure $v_n$ at $v_t$ on the

open-ended interface S and having wall-control organs capable of performing the equivalent of the functions of the source panels of $\Sigma$. The latter is, of course, a strong assumption; it means that we are testing here the principles of the AVT but not, so far as concerns wall-control organs, detailed features.

The panel-arrays used here differ from Figure 1 only in number, as follows:

Top and bottom faces: 8 panels each
Sides: 4 panels each
Front: 4 panels (as in Figure 1)

Thus, there are 28 $\Sigma$-panels and 28 field points on S.

The numerical demonstration simulates an experimental case in which the jet-flap wing with given flap angle and jet coefficient is placed in the tunnel and the tunnel started up, but at a grossly wrong free-stream angle. We assume that the energized wake lies properly within S - in other words the model's attitude in the tunnel has been adjusted to place the wake there as in Step 3 of Table II above. The simulated stream vector $\vec{U}$ is then chosen to produce the desired angle of attack, and the process of iteration is begun; we are at Step 4 of Table II.

The jet-flap-wing model of Section VI is well suited to this simulation. We begin with a free-stream vector quite different from the desired $\vec{U}$ and use our jet-flap model to give us the resulting initial wing/wake configuration and flow-field. Adopting the adaptive-wall strategy, the wall panels are activated in accordance with the algorithm (Table I). Our jet-flap model is then exercised again, this time in the presence of perturbations from the wall panels, leading to a new wing/wake configuration, and so on. If the procedure converges ($\delta v_n \to 0$), the perturbations due to wall panels are just those that cancel the errors of the initial situation, causing inner and outer fields to match at S. The outer field, it will be recalled, always satisfies the right conditions at infinity - viz. undisturbed flow at velocity $\vec{U}$. The wing/wake geometry and circulation distribution should then agree with unconfined-flow results for the same wing at the same values of $\alpha$, $\vec{U}$, and C.

The following are data taken from a typical numerical case carried through in our studies; this case constitutes the numerical demonstration for the present paper:

| | |
|---|---|
| Wing span | 4.0 |
| Wing chord including flap | 1.2 |
| Flap angle relative to wing | 60° |
| Jet-momentum coefficient | C = 0.5 |
| Desired angle of attack | $\alpha$ = 15° |
| Desired stream speed | U = 1.0 |
| Wing angle relative to tunnel axis | -45° |

Thus, the simulated stream vector $\vec{U}$ should make an angle of 60° to the tunnel axis.

Since the starting condition assumed to exist at Step 4 of Table II is quite arbitrary, let us assume for this demonstration that the wing finds itself in conditions equal to unconfined flow at U = 1.0 but at an angle of attack of 0°:

$$\text{Initial Conditions (Configuration I)} \quad \begin{cases} U = 1.0 \\ \alpha = 0° \end{cases}$$

In other words, at this point the tunnel has inadvertently been set in such a way as to simulate a free-stream vector whose angle to the tunnel axis is 45° instead of the required 60°.

The jet-flap-wing model of Section VI of this paper was used, with $\alpha = 0°$, to provide the wake geometry and circulation destribution corresponding to these initial conditions. This is called "Wing/wake Configuration 1". From these data we calculate $v_n$ and $v_t$ at the field points of S; these constitute the initial measured values of the experiment, designated $v_n^{(1)}$ and $v_t^{(1)}$. With these measured $v_t^{(1)}$'s as boundary values, we calculate the exterior flow, specifically $v_n[v_t^{(1)}]$, and form $\delta^{(1)}v_n$. Next, choosing (by experience) a suitable value of the relaxation factor k - here we choose 0.05 - we form the first improved values of $v_n$; viz.,

$$v_n^{(2)} = v_n^{(1)} + k\delta^{(1)}v_n \qquad (2)$$

These outer-flow calculations are exactly the same as would be carried out if the wind tunnel actually existed. It would be necessary, next, to adjust the wall-control organs in such a way as to produce these velocities $v_n^{(2)}$ at the field points of S. Probably the way to do this would be to measure the influence matrix, say $V_n^{(1)}{}_{ij}$, giving the effects on $v_n$ at i due to unit changes of the j-th control organ. This could be done by making a small change in the setting of each control organ and measuring the resulting changes of $v_{n_i}$.

Our procedure, for this numerical demonstration, is to simulate exactly this process: we evaluate the combined matrix $V_n^{(1)}{}_{ij}$. This requires that the strength $q_j$ of each source-panel of $\Sigma$ be increased slightly, one at a time, the jet-flap wing be iterated to convergence with consideration of the resulting velocity increments at the wing-and-wake panels, and the resulting "combined" increments in $v_{n_i}$ on S be calculated.

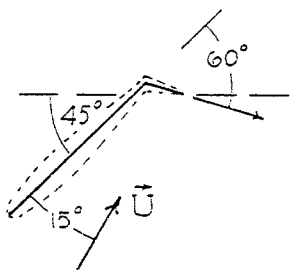

TABLE III

Outline of Numerical Simulation of Jet-Flap Wing in AVT

For given model configuration $\alpha$, C, etc. and free-stream vector $\vec{U}$:

1. Arbitrary starting situation is chosen (e.g. unconfined flow at wrong $\vec{U}$). Perturbation components $v_n^{(1)}$ and $v_t^{(1)}$ on interface are calculated (e.g. by iterating wing program for unconfined flow ($q_j^{(1)} = 0$)). This is Wing Configuration 1.

2. Outer flow is calculated: viz. $v_n[v_t^{(1)}]$ and $\delta^{(1)}v_n$.

3. "Combined" influence matrices $V_n^{(1)}{}_{ij}$ and $V_t^{(1)}{}_{ij}$ and $q_j^{(2)}$ are calculated as follows (Linearization about Wing Configuration 1):

   a. With $q_j = q_j^{(1)} + (.01,0,0,\ldots)$, wing is iterated. $V_n^{(1)}{}_{i1}$ and $V_t^{(1)}{}_{i1}$ are obtained, including "direct" effects of $q_j$.

   b. With $q_j = q_j^{(1)} + (0,.01,0\ldots)$, wing is iterated. $V_n^{(1)}{}_{i2}$ and $V_t^{(1)}{}_{i2}$ are obtained, including "direct" effects of $q_j$.

   Etc.

   c. $V_n^{(1)}{}_{ij}\,\Delta^{(1)}q_j = k\delta^{(1)}v_{n_i}$ is solved for $\Delta^{(1)}q_j$.

4. With $q_j = q_j^{(2)} = q_j^{(1)} + \Delta^{(1)}q_j$, wing is iterated, yielding Wing Configuration 2.

5. Inner flow is calculated; viz. $v_n^{(2)}$ and $v_t^{(2)}$ for Wing Configuration 2 and $q_j = q_j^{(2)}$.

6. Step 2 is repeated, yielding $v_n[v_t^{(2)}]$ and $\delta^{(2)}v_n$.

7. Step 3 is repeated, yielding new matrices $V_n^{(2)}{}_{ij}$ and $V_t^{(2)}{}_{ij}$ and $q_j^{(3)}$ (Linearization about Wing Configuration 2):

   a. With $q_j = q_j^{(2)} + (.01,0,0,\ldots)$, wing is iterated. $V_n^{(2)}{}_{i1}$ and $V_t^{(2)}{}_{i1}$ are obtained, including "direct" effects of $q_j$.

   b. With $q_j = q_j^{(2)} + (0,.01,0,\ldots)$, wing is iterated. $V_n^{(2)}{}_{i2}$ and $V_t^{(2)}{}_{i2}$ are obtained, including "direct" effects of $q_j$.

   Etc.

   c. $V_n^{(2)}{}_{ij}\,\Delta^{(2)}q_j = k\delta^{(2)}v_n$ is solved for $\Delta^{(2)}q_j$.

8. With $q_j = q_j^{(3)} = q_j^{(2)} + \Delta^{(2)}q_j$, wing is iterated, yielding Wing Configuration 3.

9. Step 5 is repeated, yielding $v_n^{(3)}$ and $v_t^{(3)}$ for Wing Configuration 3 and $q_j = q_j^{(3)}$.

Etc. to convergence.

We can now invert $V_n^{(1)}{}_{ij}$ and calculate the total changes of source strengths $q_j$ to produce the increments $k\delta^{(1)}v_n$ on S. In view of the non-linearity, the calculated matrix pertains only to "Wing/wake Configuration 1". We do not assume that our new $q_j$'s will produce exactly the $v_n$ distribution of Eq. (2) when all panels are simultaneously adjusted; hence we actually re-iterate the jet-flap wing in the presence of the velocity field of all our $\Sigma$-panels, together. The result is "Wing/wake Configuration 2". Its geometry and circulation distribution now provide the values $v_n^{(2)}{}_i$ and $v_t^{(2)}{}_i$. (The $v_n^{(2)}$'s calculates in Eq. (2) are not used further). We are now ready for the second iteration.

It will be clear to the reader that each step of the iteration of the wind tunnel toward unconfined flow involves N+1 iterative calculations of jet-flap wing properties, where N is the number of wall-control panels. This numerical simulation is therefore a rather complex one, and may be clarified by an outline of steps, as presented in Table III.

Again the Cyber 175 of the University of Arizona was used. Each "experiment" in this case required about 20 iterations in the adaptive-wall procedure. Since there were 28 $\Sigma$-panels and lateral symmetry was assumed, the process of "experimentally" determining each member of the combined $v_n$-matrix, described above, had to be carried out 14 times in each of these iteration steps - thus 15 determinations of wing geometry and flow-field were made

TABLE IV

Results of Iteration of Jet-Flap Wing to Unconfined Flow in Wind Tunnel

k = 0.05. Initial condition: $\vec{U}$ = 1.0 at 45° ($\alpha$ = 0°). Final condition: $\vec{U}$ = 1.0 at 60° ($\alpha$ = 15°).

28 Σ-panels, 28 S-points, wing centered in tunnel. C = 0.5.

| Iteration Number | $\Gamma_1$ | $\Gamma_2$ | $\Gamma_3$ | $\Gamma_4$ | $\Gamma_5$ | $\Gamma_6$ | $\Gamma_7$ | $\Gamma_8$ | $\theta_5$ | $\theta_6$ | $\theta_7$ | $\theta_8$ |
|---|---|---|---|---|---|---|---|---|---|---|---|---|
| 1 | 1.26 | 0.96 | 2.15 | 1.75 | 2.31 | 1.88 | 2.38 | 1.94 | 0.92° | 3.97° | -5.93° | 0° |
| 3 | 1.44 | 1.11 | 2.33 | 1.90 | 2.49 | 2.03 | 2.57 | 2.08 | 1.00° | 4.26° | -5.71° | 0.73° |
| 6 | 1.60 | 1.25 | 2.50 | 2.03 | 2.66 | 2.17 | 2.74 | 2.22 | 1.07° | 4.57° | -5.48° | 1.48° |
| 10 | 1.70 | 1.33 | 2.60 | 2.12 | 2.77 | 2.26 | 2.85 | 2.30 | 1.19° | 4.84° | -5.20° | 2.09° |
| 15 | 1.77 | 1.39 | 2.66 | 2.16 | 2.83 | 2.30 | 2.92 | 2.35 | 1.30° | 5.04° | -4.97° | 2.52° |
| 20 | 1.80 | 1.41 | 2.69 | 2.18 | 2.86 | 2.33 | 2.95 | 2.37 | 1.36° | 5.16° | -4.84° | 2.74° |
| 30 | 1.82 | 1.43 | 2.72 | 2.20 | 2.89 | 2.34 | 2.97 | 2.39 | 1.40° | 5.24° | -4.73° | 2.92° |
| Unconfined | 1.86 | 1.46 | 2.73 | 2.20 | 2.90 | 2.34 | 2.98 | 2.37 | 2.18° | 6.02° | -3.31° | 4.59° |

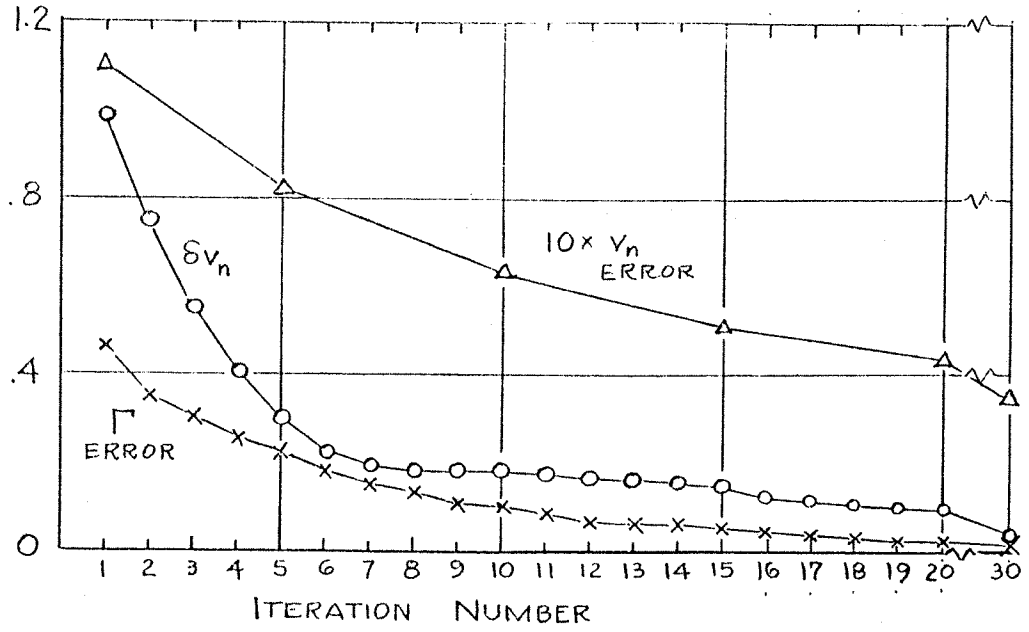


FIGURE 5 - Iteration of jet-flap wing to unconfined flow in wind tunnel. k = 0.05. 28 Σ-panels, 28 points on S. Initial condition: $\vec{U}$ = 1.0 at 45° ($\alpha$ = 0°). Final condition: $\vec{U}$ = 1.0 at 60° ($\alpha$ = 15°). x average absolute error in $\Gamma_r$. o maximum $\delta v_n$ on S. Δ average absolute true error in $v_n$ on S. (The points are connected only for clarity). C = 0.5

in each iteration step. Each of these determinations required at least 7 iterations of the wing geometry. Nevertheless, a typical "experiment" was carried out, from arbitrary starting situation to unconfined flow, in about a minute of computer time.

Results of this calculation are presented in Fig. 5 and Table IV. In Fig. 5 are plotted (i) the mean absolute error in $\Gamma_r^{(p)}$, (ii) the maximum absolute value of the "mismatch-signal" $\delta^{(p)}v_n$ on S, and (iii) the average absolute error in $v_n^{(p)}$ on S. The abscissa is the iteration-number, p. As has already been mentioned in connection with Figure 2, the errors in (i) and (iii) can be evaluated at any step of the iteration in this test case because the properties and flow-field of the jet-flap wing in unconfined flow are known.

It will be noted that the circulations of the various wing and wake panels, including the total lift (approximately proportional to the mean of $\Gamma_7$ and $\Gamma_8$ in this case), converge rapidly to a close approximation to unconfined-flow values. This means that the aerodynamic properties of the wing are accurately rendered. This occurs in spite of the rather slow convergence of $\delta v_n$ toward zero and the persistence of an appreciable error in the flow field at interface S.

## VIII. Additional Simulations

Following this successful simulation of the jet-flap-wing model, a number of additional, related, numerical experiments were carried out; some of which will be summarized briefly here.

Mean-square fitting:

The tunnel model employed in Section VII, above, had 28 wall-control panels and 28 instrument locations (field points), as mentioned. Simulations were also carried out using the same array of 28 $\Sigma$-panels (wall-control panels) together with 44 field points on S, as in Figure 1. When the number of field points (say 44) exceeds the number of $\Sigma$-panels (say 28); the 28 panel strengths q are made to fit the 44 boundary values $v_n$ in a best-mean-square sense. Thus, it would be expected that the iteration procedure would lead to a better approximation to unconfined flow than given by a 28 x 28 model (but perhaps poorer than 44 x 44). The results of this experiment are presented, below, in Table V. The expected improvement of results was observed.

It will be noted that a larger k was used here than in Table IV; this was found to be possible when mean-square fitting was used. uns were made with this (44 x 28) array with k equal to 0.15, 0.2, and 0.3. Most rapid convergence seemed to occur with k = 0.3. Slightly more accurate results, as measured by the average absolute error of $\Gamma_r$, occurred with k = 0.20.

Improved convergence and Dowell's formulas:

The use of a relaxation factor k that is uniform in space and also constant during the process of iteration is quite arbitrary. Various guesses have been made, during this research, as to what changes of k might accelerate convergence and/or improve final results. Our conclusion has been, to date, that convergence is accelerated if k is increased as the iteration is carried out. For example, in one run, k was put equal to 0.10 for the first 10 iterations, then increased by 0.01 in each subsequent iteration, to a value of 0.20 in the 20th step. The process converged appreciably faster than with k = 0.10, 0.15, or 0.20. This run is included in Table V.

Dowell[12] has shown how the unconfined-flow values of $v_n$, $v_t$, and the wall-panel strengths q can be calculated in one step from the measured $v_n^{(1)}$ and $v_t^{(1)}$, for a linear system. Although the present

Table V

Results of Additional Simulations: Jet-Flap Wing in Wind Tunnel

Initial Condition: $|\vec{U}| = 1.0$ ($\alpha$=0°). Final Condition: $|\vec{U}| = 1.0$ ($\alpha$=15°).

Number of $\Sigma$-panels = 28. C = 0.5

| Stream inclination Initial | Final | Number of field points | k | $\lvert\delta v_n\rvert$ max | Average abs. error in $\Gamma_r$ | Average abs. error in $v_n$ on S | Number of iterations |
|---|---|---|---|---|---|---|---|
| Model: Wing only. Position: centered | | | | | | | |
| 45° | 60° | 28 | 0.05 | 0.039 | 0.0055 | 0.0368 | 30 |
| 45° | 60° | 44 | 0.15 | 0.113 | 0.0055 | 0.0488 | 25 |
| 45° | 60° | 44 | 0.20 | 0.133 | 0.0033 | 0.0447 | 15 |
| 45° | 60° | 44 | 0.30 | 0.115 | 0.0035 | 0.0510 | 15 |
| 45° | 60° | 44 | Varied: .1 to .2 | 0.115 | 0.0053 | 0.0483 | 20 |
| Model: Wing and tail. Position: centered | | | | | | | |
| 45° | 60° | 28 | 0.05 | 0.145 | 0.0251 | 0.0532 | 15 |
| 30° | 45° | 28 | 0.05 | 0.134 | 0.0119 | 0.0618 | 15 |
| Model: Wing and tail. Position: raised ⅓ span | | | | | | | |
| 30° | 45° | 28 | 0.05 | 0.110 | 0.0090 | 0.0499 | 18 |
| 15° | 30° | 28 | 0.05 | 0.114 | 0.0081 | 0.0610 | 18 |

problem is nonlinear (because wake geometry depends on the solution), trial have been made using his procedure. This involves the influence matrices of both outer and inner flows; the former is used in Steps 2, 6, etc. of Table III and does not change. The latter is calculated for "Wing Configuration 1" in Step 3. It has been found that unconfined-flow values based on Dowell's formulas and using these matrices are very close to those obtained by iteration. This means, of course, that the inner-flow matrix does not change much during the iteration for this particular wing-model, and that an important simplification is achieved.

Two remarks seem appropriate at this point: (1) that the success of Dowell's procedures in any case is ascertained by evaluating $\delta v_n$, and (2) that if this test fails - i.e., if the resulting $\delta v_n$'s are not as small as desired - the matrix can be re-calculated and a second step taken. That is, Dowell's procedure can always be used in an iterative way if necessary, and important savings of time can still be achieved in comparison with simple-minded iteration using a relaxation factor k.

Model with horizontal tail surface:

Runs were also made in which a typical horizontal tail surface was modelled together with the wing. This surface was modelled as a simple horse-shoe vortex carrying a down-load, located 1/2-span behind the wing. The tail span was chosen to be half that of the wing. The circulation of this horse-shoe vortex is denoted by $\Gamma$ the procedures of Sections VI and VII were extended to include this variable, whose magnitude was determined by the total perturbation velocity at the tail position. It will be seen that the horizontal tail had only minor effects on $\Gamma_1$, ..., $\Gamma_8$ and the wake configuration.

Changes of wing location and stream inclination:

The central idea of the AVT is to place the wake so that it does not impinge on the instrument array (S). This can be accomplished in a variety of ways: there is a range of stream inclinations (arg $\vec{U}$) within which the wake, for any wing configuration, lies somewhere between the top and bottom surfaces of the interface S as it leaves the working section downstream. This range can be increased by placing the model higher in the tunnel. In Table V are listed the results of four runs made to explore this idea. The wing-plus-tail model was employed in these simulations. It will be seen that only very small changes resulted; hence model height can be maximized and stream inclination minimized, in order to accommodate cases of extreme wake deflection, without impairing the accuracy of the tunnel.

## Concluding Remarks

On the basis of the numerical simulations reported here, it appears that a tunnel of AVT type can be used to test high-lift configurations, correcting for gross errors in starting conditions and arriving at conditions closely approximating unconfined flow. Since the simulations carried out make no pretense of modelling in detail the properties of real wall-control organs, no further conclusions can be drawn until the program is moved into the realm of laboratory experiments.

This work has been supported at the University of Arizona by the O.N.R. under Contract N 00014-79-C-0010. The encouragement and technical advice received from Morton Cooper are gratefully acknowledged. The author also acknowledges the able assistance of Karl Allmendiger and Daniel C.L. Lee, graduate assistants at the University of Arizona. This research team is now proceeding toward the construction and testing of a demonstration version of the AVT.

## References

1. Ferri, A., and Baronti, P., "A Method for Transonic Wind Tunnel Corrections," AIAA J., Vol. 11, Jan. 1973, pp. 63-66.

2. Sears, W. R., "Self-Correcting Wind Tunnels," (The Sixteenth Lanchester Memorial Lecture), Aeronautical J., Vol. 78, Feb/March 1974, pp. 80-89.

3. Sears, W. R., Vidal, R. J., Erickson, J. C. Jr., and A. Ritter, "Interference-Free Wind-Tunnel Flows by Adaptive-Wall Technology," J. of Aircraft, Vol. 14, No. 11, November 1977, pp. 1042-1050.

4. Satyanarayana, B., Schairer, E., and Davis, S., "Adaptive-Wall Wind-Tunnel Development for Transonic Testing," J. of Aircraft, Vol. 18, No. 4, April 1981, pp. 273-279.

5. Spence, D. A., "The Lift Coefficient of a Thin, Jet-Flapped Wing," Proceedings of the Royal Society, Vol. A238, Dec. 1956, pp. 46-68.

6. Maskell, E. C., and Spence, D. A., "A Theory of the Jet Flap in Three Dimensions," Proceedings of the Royal Society, Vol. A251, June 1959, pp. 407-425.

7. Kerney, K. P., "An Asymptotic Theory of the High-Aspect-Ratio Jet Flap," Ph.D. Thesis, Graduate School of Aeronautical Engineering, Cornell University, 1967.

8. Tokuda, N., "An Asymptotic Theory of the Jet Flap in Three Dimensions," Journal of Fluid Mechanics, Vol. 46, Pt. 4, 1971, pp. 705-726.

9. Addessio, F. L., and Shifstad, J. G., "Aerodynamics of a Finite Aspect Ratio Jet Flap at Low Flight Speeds," Journal of Aircraft, Vol. 14, No. 10, October 1977, pp. 936-943.

10. Maskew, B., "A quadrilateral vortex method applied to configurations with high circulation," NASA SP-405, 1976, pp. 163-186.

11. Lee, Daniel C.L., "The Modelling of a High-Lift Jet-Flapped Wing," Master of Science Report, Department of Aerospace and Mechanical Engineering, University of Arizona, Tucson, Arizona, 1981.

12. Dowell, E. H., "Control Laws for Adaptive Wind Tunnels," AIAA J., Vol. 19, Nov. 1981, pp. 1486-1488.